Available online at www.sciencedirect.com
ScienceDirect
Journal of Organometallic Chemistry 691 (2006) 5312–5325
Journal of Organometallic Chemistry
www.elsevier.com/locate/jorganchem

Mechanistic comparison of ruthenium olefin metathesis catalysts: DFT insight into relative reactivity and decomposition behavior

Werner Janse van Rensburg [a,*], Petrus J. Steynberg [a], Megan M. Kirk [a], Wolfgang H. Meyer [a], Grant S. Forman [b]

[a] Sasol Technology (Pty), Ltd., R&D Division, 1 Klasie Havenga Road, Sasolburg 1947, South Africa
[b] Sasol Technology (UK), Ltd., Purdie Building, North Haugh St. Andrews, Fife KY16 9ST, Scotland, UK

Received 30 June 2006; received in revised form 19 August 2006; accepted 19 August 2006
Available online 1 September 2006

Abstract

The reaction mechanism and substrate-induced decomposition behavior of three ruthenium olefin metathesis catalysts, viz. first- and second-generation catalysts and the recently developed Phoban catalyst (“Phobcat”) are compared by constructing ΔG surfaces at 298.15 K and 1 atm for the complete ligand systems. From these calculations fundamental insight is gained into the reactivity and stability observed experimentally for the three catalysts. In particular, the higher conversions obtained for the first-generation derived Phobcat catalyst, compared to conventional first-generation catalysts, is attributed to its similarity to the second-generation catalysts instead of first-generation catalyst. Important differences between the calculated ΔG surfaces and previously reported total electronic energy (ΔE) surfaces for the metathesis mechanism with complete ligand complexes are discussed.
© 2006 Elsevier B.V. All rights reserved.

Keywords: Metathesis; DFT; Mechanism; Decomposition; Phoban catalyst

1. Introduction

The development of Ru-alkylidene complexes as catalysts for olefin metathesis has received considerable attention in recent years due to its versatility in organic synthesis and polymer chemistry [1]. The awarding of the 2005 Nobel Prize in Chemistry to Yves Chauvin, Richard R. Schrock and Robert H. Grubbs for the development of the metathesis method in organic synthesis recognizes the importance and versatility of metathesis as a powerful tool in many chemistry applications [2]. In particular, the ruthenium catalysts $[(PCy_3)_2Cl_2Ru{=}CHPh]$ [3] (**I**) and $[(H_2IMes)(PCy_3)Cl_2Ru{=}CHPh]$ [4] (**II**), commonly referred to as the first- and second-generation Grubbs catalysts, form the cornerstone of many metathesis applications such as ring-closing metathesis (RCM), cross-metathesis (CM) and ring-opening polymerization (ROMP) [5]. In contrast to their successful use in organic synthesis, the application of first- and second-generation catalysts on the commodity industrial scale has not too date been successfully demonstrated. For example, the self-metathesis (SM) of linear unfunctionalized α-olefins catalyzed by first-generation catalysts display relatively poor life times at temperatures above 50 °C [6]. Although the second-generation systems display enhanced activity and thermal stability relative to first-generation catalysts, the formation of secondary metathesis products (SMPs) under certain circumstances can be a significant cause of low selectivities in these systems [7–9]. In an attempt to alleviate these concerns and to improve catalyst life time, we have recently reported on three different approaches: (i) The development of a new first-generation Phoban catalyst, “Phobcat”, [(Phoban-Cy)$_2$Cl$_2$ Ru=CHPh][6] (**III**), bearing Phoban-Cy {9-cyclohexyl-9-phosphabicyclo-[3.3.1]-nonane} instead of tricyclohexylphosphine as ligands (Fig. 1), which exhibits significant improved

* Corresponding author. Tel.: +27 16 960 4716; fax: +27 11 522 0295.
E-mail address: Werner.JansevanRensburg@sasol.com (W.J. van Rensburg).

0022-328X/$ - see front matter © 2006 Elsevier B.V. All rights reserved.
doi:10.1016/j.jorganchem.2006.08.075

stability and conversion compared to traditional first-generation catalysts. (ii) The improvement of first-generation catalyst efficiency by addition of phenols [10]. (iii) Enhanced performance of first-generation catalysts upon addition of tin and iron halogenides [11].

The broad interest in Ru-alkylidene catalyzed olefin metathesis applications have spurred a number of fundamental studies, both experimentally [12–18] and theoretically [19–32], aimed at elucidating the most appropriate mechanistic sequences in the metathesis cycle and the identification of the relevant active intermediates. From these studies variations of the Chauvin mechanism [33] are commonly accepted in which initiation, by dissociation of a phosphine ligand from the 16*e* Ru(II) catalyst precursor (**1**, Scheme 1), is followed by coordination of an olefinic substrate to the unsaturated 14*e* Ru-species (**2**) affording the π-complex **3**. Subsequent oxidative [2+2] cycloaddition results in the formation of a Ru(IV) ruthenacyclobutane intermediate (**4**) from which the liberation of olefinic product and formation of Ru-carbene intermediate follows after reductive elimination in a productive metathesis sequence.

Despite the wide interest and progress in unraveling the metathesis mechanism the fundamentals of catalyst decomposition is only addressed in a few experimental studies [34–37]. In particular, thermal decomposition of first- and second-generation catalyst systems play a significant role in inhibition of catalyst turnover numbers, while decomposed ruthenium complexes may contribute to detrimental side reactions such as olefin isomerization. A bimolecular decomposition route was found to be favored by substituted ruthenium-alkylidenes, such as the propylidene $(PCy_3)_2(Cl)_2Ru{=}CHCH_2CH_3$ [34], from which the formation of *trans*-3-hexene is observed at 55 °C. The formation of face-bridged dimers from the alkenylidene precursor $(dcypb)(Cl)_2Ru{=}CHCH{=}CMe_2$ [dcypb = 1,4 -bis(dicyclohexylphosphino)butane] was also put forward as evidence that this transformation may account for decomposition of the Grubbs catalyst $(PPh_3)_2Cl_2Ru{=}CHCH{=}CMe_2$ [37]. In contrast to this bimolecular alkylidene decomposition route the decomposition of methylidene complexes, such as $(PCy_3)_2(Cl)_2Ru{=}CH_2$, were found to favor a unimolecular decomposition route involving incorporation of methylidene hydrogens into the phosphine ligands of the decomposition products [34]. Attack of a phosphine ligand on a Ru-carbene carbon, to form $[R'\text{-}PR_3]^+X^-$ species, was also recently proposed to represent a mode of catalyst decomposition [35]. The decomposition routes indicated above are relevant for catalyst systems in the absence of substrate. It is, however, conceivable that interaction of the substrate olefin with Ru-carbene species could open up new decomposition pathways [23]. In particular, we [38] have recently shown for the first time that the formation of propene during the degenerate Ru-methylidene catalyzed metathesis of ethylene causes irreversible substrate-induced decomposition of the Ru-carbene functionality. This was subsequently also demonstrated by others [39]. The mechanism for this decomposition sequence (Scheme 1) is thought to involve the formation of a Ru(IV) allyl-hydride species (**5**) after β-hydride transfer in the ruthenacyclobutane precursor (**4**) [40,41]. Subsequent reductive transfer of the hydride in **5** to the terminal position of the allylic fragment results in the formation of a coordinatively unsaturated Ru(II) complex (**6**) which is inactive for metathesis.

In the current study, DFT calculations are employed to compare the basic mechanistic steps for olefin metathesis catalyzed by a first- (**I**) and second-generation (**II**) catalyst, as well as the newly developed Phobcat $[Cl_2(Phoban\text{-}Cy)_2Ru{=}CHPh]$ (**III**) catalyst. The primary aim of these studies is to calculate the complete Gibbs free energy surface at 298.15 K and 1 atm for the catalysts with complete ligands, i.e. PCy_3 for **I**, PCy_3 and IMes for **II** and Phoban-Cy for **III**. Despite the large theoretical interest in the mechanism of first- and second-generation catalyzed metathesis the studies focus, to the best of our knowledge, either on strip-down models [19,20], both with and without ΔG corrections, or relevant complete models without ΔG corrections [23–29]. In a small number of metathesis related theoretical studies [31] ΔG corrections are included for complete model systems, but these studies are not focused on a basic metathesis mechanistic comparison

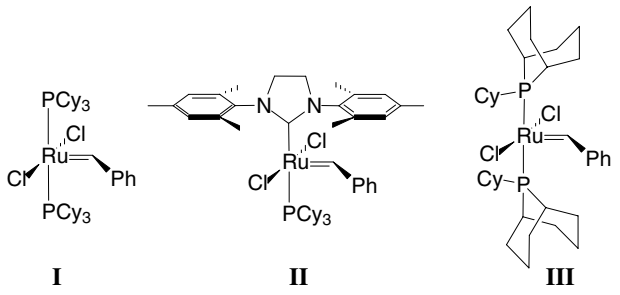

Fig. 1. Structures of first- (**I**) and second-generation (**II**) Grubbs and Phoban (**III**) catalyst precursors.

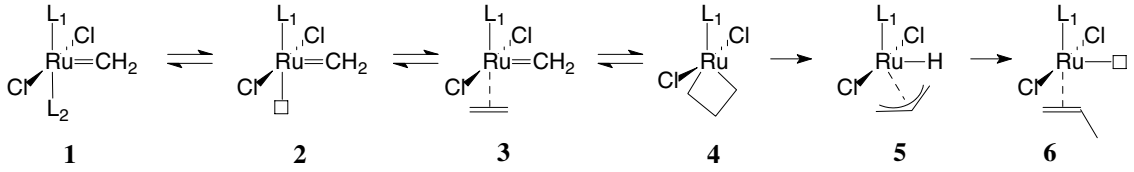

Scheme 1. The dissociative mechanistic sequence and substrate-induced decomposition of the ruthenacyclobutane intermediate with ethylene and methylidene as respective model olefin and alkylidene species.

between first- and second-generation catalysts. Secondly, calculation and comparison of the Phobcat catalyzed metathesis mechanism with the mechanisms for first- and second-generation catalysts should provide fundamental insight into the unique catalytic behavior observed for Phobcat. To the best of our knowledge no theoretical mechanistic studies have yet been performed on this unique catalyst system. Thirdly, our recently reported [38] substrate-induced decomposition mechanism is also studied for Phobcat aiming to gain insight into its superior stability during catalysis compared to conventional first-generation catalysts.

2. Computational details and models

All geometry optimisations were performed with the DMOL^3 density functional theory (DFT) code [42] as implemented in the MaterialsStudio™ (Version 3.2) program package of Accelrys Inc. The non-local generalized gradient approximation (GGA) exchange-correlation functional by Perdew and Wang (PW91) [43] was used for all geometry optimisations. This functional was previously used by us with success with ruthenium [10,38,44] and other transition metals [45]. The convergence criteria for these optimisations consisted of threshold values of 2×10^{-5} Ha, 0.00189 Ha/Å and 0.00529 Å for energy, gradient and displacement convergence, respectively, while a self consistent field (SCF) density convergence threshold value of 1×10^{-6} Ha was specified. DMOL^3 utilizes a basis set of numeric atomic functions, which are exact solutions to the Kohn–Sham equations for the atoms [46]. These basis sets are generally more complete than a comparable set of linearly independent Gaussian functions and have been demonstrated to have small basis set superposition errors [46]. In the present study, an all electron polarized split valence basis set, termed double numeric polarized (DNP) has been used. All geometry optimisations employed highly efficient delocalised internal coordinates [47]. The use of delocalized coordinates significantly reduces the number of geometry optimisation iterations needed to optimise larger molecules compared to the use of traditional Cartesian coordinates.

All the geometries optimised were also subjected to full numerical frequency analyses at the same GGA/PW91/DNP level of theory to verify the nature of all stationary points. Equilibrium geometries were characterised by the absence of imaginary frequencies. Preliminary transition state geometries were obtained by either the DMOL^3 *PES scan* functionality or the integrated linear synchronous transit/quadratic synchronous transit (*LST*/*QST*) algorithm available in MaterialsStudio™. These preliminary structures were then subjected to full TS optimisations using an eigen vector following algorithm. All transition structure geometries exhibited only one imaginary frequency in the appropriate reaction coordinate. All reported energies refer to Gibbs free energy corrections to the total electronic energies at 298.15 K and 1 atm, with the inclusion of zero-point energy (ZPE) corrections, in the gas phase. Although the relative Gibbs free energies calculated in the gas phase may not directly be correlated with the expected relative Gibbs free energies in solution, the gas phase values reported are still deemed appropriate for relative comparison of different catalyst systems within the scope of the current study.

Only complete ligand systems were considered for the catalyst models in the current study. For the first-generation catalyst (**I**) tricyclohexylphosphine (PCy_3) was used, while a combination of PCy_3 and the unsaturated N-heterocyclic carbene, IMes (Mes = 2,4,6-trimethylphenyl), was used as ligands for the second-generation catalyst. For the remainder of this paper the numbering **II** thus refer to the IMes ligand and not the H_2IMes ligand as referred to in the introduction. The third catalyst is based on the first-generation catalyst, but the PCy_3 ligands were replaced with 9-cyclohexyl-9-phosphabicyclo-[3.3.1]-nonane as ligand as illustrated for **III**. Abbreviated reference to this ligand in the text is either cyclohexyl-[3.3.1]-phoban or Phoban-Cy. The catalyst itself is referred to as Phobcat to distinguish it from the traditional first- and second-generation catalysts. Ethylene was used as model olefinic substrate in combination with a methylidene functionality on ruthenium throughout this study, effectively allowing for the description of degenerate etyhylene metathesis. For the Phobcat catalyst two isomeric catalytic species were considered, numbered as **III** and **III′**, respectively. The catalyst **III** refer to a top Phoban-Cy ligand with the Cy group orientated *transoid* with respect to the methylidene fragment, while **III′** refer to a Cy group with *cisoid* orientation with respect to the methylidene fragment. The numbering scheme **I**, **II**, **III**, and **III′** are consistently used throughout the text in combination with the species numbered **1-6** in Scheme 1 to clearly distinguish the different structures.

3. Results

3.1. Catalyst initiation

It is commonly accepted that the Ru-catalyzed olefin metathesis reaction proceeds via a dissociative mechanism, involving dissociation of one ligand prior to olefin coordination. In this sense catalyst initiation involves the dissociation of PCy_3, for both the first and second-generation catalysts, and Phoban-Cy for Phobcat. The methylidene CH_2 plane of the precatalyst complex, **1**, may be orientated either parallel (**1a**) or perpendicular (**1b**) to the Cl–Ru–Cl plane, as illustrated in Fig. 2.

No stationary point could successfully be located for the first-generation precatalyst complex, **I-1**, in which the CH_2 plane is orientated parallel to the Cl–Ru–Cl plane (**I-1a**); all optimisation attempts resulted in spontaneous rotation of the methylidene moiety toward a perpendicular orientation (**I-1b**). However, the relative electronic energy (ΔE) of **1a** is estimated to be higher than **1b** by ~6 kcal/mol, as

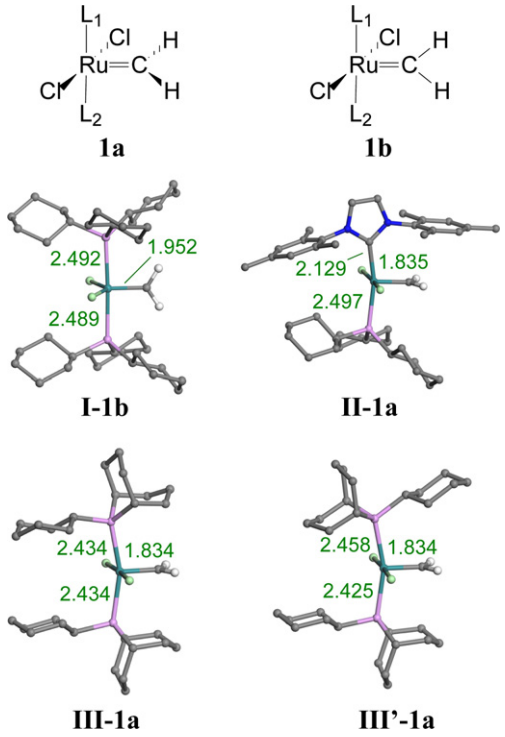

Fig. 2. Potential Ru-methylidene complexes for **1a** and **1b**, along with the optimized geometries for the lowest energy first- and second-generation and Phobcat catalyst precursor complexes. The hydrogen atoms on the ligands are omitted for clarity and the unit of the indicated bond distances is angstrom (Å).

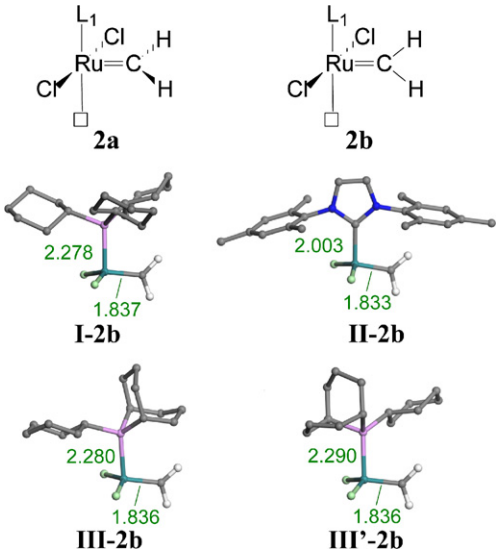

Fig. 3. Potential Ru-methylidene complexes for **2a** and **2b**, along with the optimized geometries for the lowest energy first- and second-generation and Phobcat unsaturated complexes. The hydrogen atoms on the ligands are omitted for clarity and the unit of the indicated bond distances is angstrom (Å).

determined from the flattening of the potential energy surface (PES) in the reaction coordinate: **I-1a** → **I-1b**. A structure corresponding to **I-1a**, instead of **I-1b**, was used in construction of a potential energy surface for the first-generation catalyzed metathesis sequence with ethylene as substrate in a recent DFT study by Adlhart and Chen [28].

In contrast, the parallel orientated methylidene complexes for the second-generation (**I-1a**) and Phobcat (**III-1a** and **III′-1a**) catalysts were not only successfully located, but were also found to be lower in energy than the corresponding perpendicular orientated methylidene complexes **II-1b**, **III-1b** and **III′-1b**, respectively. In particular, vibrational analyses on the optimized geometries for **II-1b**, **III-1b** and **III′-1b** revealed one imaginary frequency for each of the three structures with normal modes corresponding to transition structures (TS) for **II-1b** → **II-1a** ($77i\ \mathrm{cm}^{-1}$; $\Delta G_{298} = -2.9$ kcal/mol), **III-1b** → **III-1a** ($53i\ \mathrm{cm}^{-1}$; $\Delta G_{298} = -6.4$ kcal/mol) and **III′-1b** → **III′-1a** ($40i\ \mathrm{cm}^{-1}$; $\Delta G_{298} = -6.8$ kcal/mol), respectively. From the four lowest energy catalyst precursor complexes illustrated in Fig. 2 it is thus evident that different methylidene orientations account for the most stable precatalyst complexes.

In the dissociative metathesis mechanism ligand dissociation proceeds prior to the interaction of olefin with ruthenium. Consequently, catalyst initiation requires the formation of unsaturated 14*e* complexes, **2** (Scheme 1). Once again, different orientations of the methylidene model complexes are possible for the three catalysts under investigation as illustrated in Fig. 3.

No stationary points corresponding to parallel orientation of the methylidene moiety with respect to the Cl–Ru–Cl plane (**2a**) were successfully located for any of the catalysts. In all cases spontaneous formation of the perpendicular methylidene orientation (**2b**) resulted during optimization, irrespective of the starting methylidene orientation. The four optimized geometries important in the current study are also illustrated in Fig. 3 along with selected bond distances (Å).

3.2. Ethylene coordination and ruthenacyclobutane formation

Ethylene coordination to the unsaturated intermediate species, **2**, results in the formation of the corresponding π-complexes **3**. In theory four different structures should be possible, for ethylene coordination *trans* to the ligand, for each of the catalytic systems under investigation, as illustrated in Fig. 4: (i) ethylene coordinated parallel to the Ru=C bond and the CH_2 plane parallel to the Cl–Ru–Cl plane (**3a**), (ii) ethylene coordinated parallel to the Ru=C bond and the CH_2 plane perpendicular to the Cl–Ru–Cl plane (**3b**), (iii) ethylene coordinated perpendicular to the Ru=C bond and the CH_2 plane parallel to the Cl–Ru–Cl plane (**3c**) and (iv) ethylene coordinated perpendicular to the Ru=C bond and the CH_2 plane perpendicular to the Cl–Ru–Cl plane (**3d**).

All four structures illustrated in Fig. 4 were successfully optimized for the *first-generation* catalyst system. The relative ΔG_{298} energies (kcal/mol) calculated for these complexes in increasing order are: **I-3b** (0.0) < **I-3d** (1.3) < **I-3a**

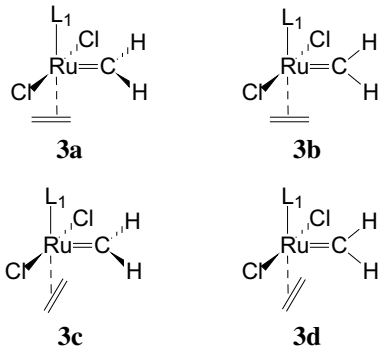

Fig. 4. Four possible combinations for ethylene and methylidene hydrogen orientations.

(4.6) < **I-3c** (7.7). Therefore, the most appropriate first-generation ethylene complex to consider in the construction of the free energy surface should have ethylene parallel to the Ru=C bond and the CH_2 plane perpendicular to the Cl–Ru–Cl plane. In contrast, an ethylene π-complex corresponding to **I-3c** was considered in the theoretical construction of a potential energy surface in a recent account [28].

For the *second-generation* catalyst only three stationary points for ethylene coordination were successfully located, viz. **II-3b**, **II-3c** and **II-3d**. Whereas **II-3c** and **II-3d** were established from vibrational analyses to be true equilibrium structures, **II-3b** was found to resemble a TS structure with normal mode ($30i\,cm^{-1}$) corresponding to methylidene rotation from perpendicular to parallel relative to the Cl–Ru–Cl plane. All attempts to optimize a structure corresponding to **II-3a** resulted in the spontaneous formation of the corresponding ruthenacyclobutane complex **II-4**. However, an estimate of the electronic energy (ΔE) of **II-3a**, relative to **II-3b**, **II-3c** and **II-3d**, was obtained from the flattening of the PES for **II-3a** → **II-4** optimization prior to the formation of **II-4**, resulting in a relative energy (kcal/mol) trend of **II-3a** (∼0.0) < **II-3c** (0.9) < **II-3d** (4.0) < **II-3b** (5.3). It is thus evident that the ethylene coordination mode resembled by the **II-3a** estimate represents the lowest energy second-generation methylidene ethylene complex, proceeding essentially without barrier to the corresponding ruthenaccylobutane complex, **II-4**, on the ΔE potential energy surface. This may provide preliminary insight into the relative reactivity of the second-generation catalyst system (vide infra).

The calculated relative energies of methylidene ethylene isomers for *Phobcat*, **III-3** and **III′-3**, revealed similar trends. Similar to the results obtained for the second-generation catalyst only three equilibrium stationary points were successfully optimized for both the Phobcat systems, viz. **3b**, **3c** and **3d**. Attempts to optimize **III-3a** and **III′-3a** both resulted in the spontaneous formation of a single ruthenacyclobutane isomer, **III-4** [48]. Once again, a rough estimate for the relative electronic energies (ΔE) of **III-3a** and **III′-3a** may only be obtained by the relative flattening of the optimization PES's prior to the formation of **III-4**. The calculated relative electronic energies (kcal/mol) are: **III-3c** (0.0) < **III-3d** (0.5) < **III-3b** (0.8) < **III-3a** (∼1.9) and **III′-3c** (0.0) < **III′-3a**(∼1.4) < **III′-3b** (1.6) < **III′-3d** (2.0). It is evident that the lowest energy methylidene ethylene complexes correspond to methylidene protons parallel to the Cl–Ru–Cl plane and ethylene coordinated perpendicular to the Ru=C bond, i.e. structures **III-3c** and **III′-3c**.

It is thus interesting to note that for the three catalysts considered in the current study different relative ethylene/methylidene orientations constitute the lowest energy Ru-ethylene π-complexes in each case. These lowest energy complexes are considered the most relevant precursor structures for ruthenacyclobutane formation, the optimized structures of which are illustrated in Scheme 2, along with the located transition states for transformation of **3-4** for the relevant catalytic species. Although not clearly discernable in Scheme 2, significant rotation of the methylidene unit in **TS-I-3b-4** ($98i\,cm^{-1}$), as well as the ethylene moieties in **TS-III-3c-4** ($50i\,cm^{-1}$) and **TS-III′-3c-4** ($106i\,cm^{-1}$), form part of the single imaginary normal modes for the respective transition state structures.

3.3. Ruthenacyclobutane decomposition

Apart from degenerate ethylene metathesis via the ruthenacyclobutane intermediate **4** an alternative decomposition route was recently shown by us to also involve the ruthenacyclobutane intermediate for the formation of propylene as major decomposition product [38]. Mechanistically this involves two steps from the ruthenacyclobutane: β-hydride transfer from the metallacycle to yield the allyl hydride species **5**, followed by hydride transfer to a terminal allyl methylene to yield the metathesis inactive propylene π-complex **6**. Although the optimized stationary points for this substrate-induced decomposition sequence for first- and second-generation ethylene methylidene complexes were reported before [38], they are again illustrated in Scheme 3 to afford direct comparison with the corresponding decomposition structures for the Phobcat models.

Scheme 3 illustrates a few interesting differences between the optimized geometries when direct comparisons are made among the relevant catalyst models. The β-hydride transfer transition state structures for the second-generation catalyst (**TS-II-4-5**) and Phobcat models (**TS-III-4-5** and **TS-III′-4-5**) are geometrically very similar as is evident from the respective C_{NHC}–Ru–C (118.9°) and P–Ru–C (119.8° and 119.1°) angles. In contrast, the corresponding P–Ru–C angle for the first-generation transition state (**TS-I-4-5**) is calculated at 96.1°. These differences further result in different reaction coordinates for the transferring hydride for the first-generation catalyst compared to the second-generation and Phobcat models, effectively proceeding to allyl hydride complexes, **5**, with different relative allyl and hydride orientations. Whereas these relative differences in transition states for allyl formation impacts on the relative energies of the corresponding barriers (vide infra), the second, propene generating hydride transfer steps (**5** → **6**), proceed with similar geometrical parameters

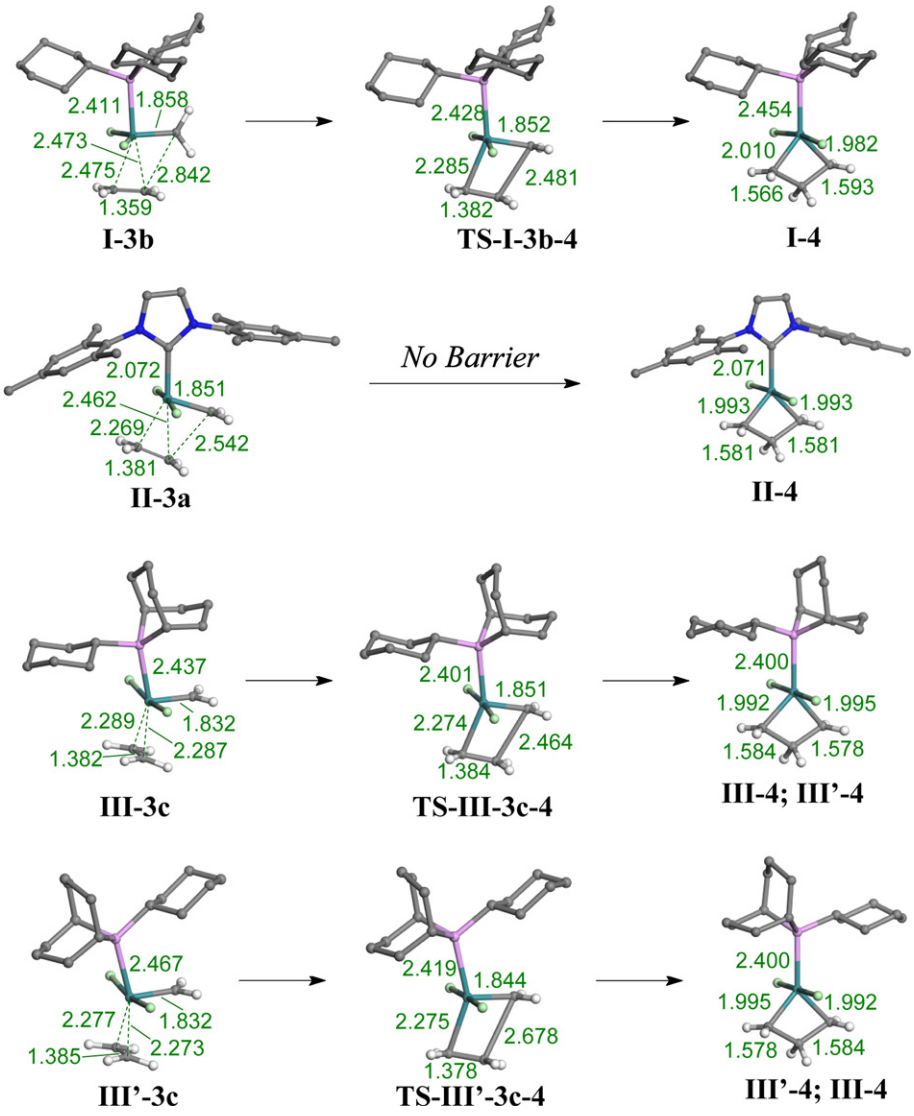

Scheme 2. Optimized geometries of the lowest energy equilibrium and transition state structures involved in the transformation of methylidene ethylene π-complexes (**3**) to the corresponding ruthenacyclobutane (**4**) intermediate complexes for the first- and second-generation and Phobcat catalyst systems. The selected bond lengths are in angstrom (Å) and hydrogen atoms on the ligands are omitted for clarity.

for all the catalyst models considered. The propylene coordination complexes, **6**, are unlikely to be active for metathesis and most likely represent precursor complexes for further decomposition pathways.

3.4. Free energy surface

The relative energies for all optimized structures discussed in the current paper are summarized in Table 1. The energies of the lowest energy precatalyst complexes for the first-generation (**I-1b**), second-generation (**II-1a**) and Phobcat (**III-1a**) catalysts are set to zero in each case, with all other relative energies balanced with the energies of free phosphine ligand and free ethylene where necessary. Both the relative ΔE and ΔG_{298} energies are summarized in Table 1, affording smooth comparison of relative changes to the ΔE surfaces upon correcting toward ΔG_{298} surfaces.

Whereas most relative energies presented in Table 1 naturally follows from the structures presented in the preceding sections, the ΔG_{298} energy estimates for ethylene coordination and cyclization for the second-generation catalyst needs further elaboration. From relative ΔE energies it was found that the ethylene π-complex, **II-3a**, represents the lowest energy structure. However, **II-3a** is not a true equilibrium structure due to its spontaneous optimization to the ruthenacyclobutane complex **II-4**. Due to the relatively low electronic energy for **II-3a**, however, the ΔG_{298} corrections for this mode of ethylene interaction with ruthenium was estimated according to the ΔG_{298} corrections found for formation of the alternative true equilibrium structure **II-3c**, which has a similar parallel orientation of CH_2 plane with respect to the Cl–Ru–Cl plane. Therefore, the ΔG_{298} estimate for **II-3a** is calculated as follows: $\Delta G_{298}(\mathbf{II\text{-}3a}) = \Delta E(\mathbf{II\text{-}3a}) - [\Delta E(\mathbf{II\text{-}3c}) -$

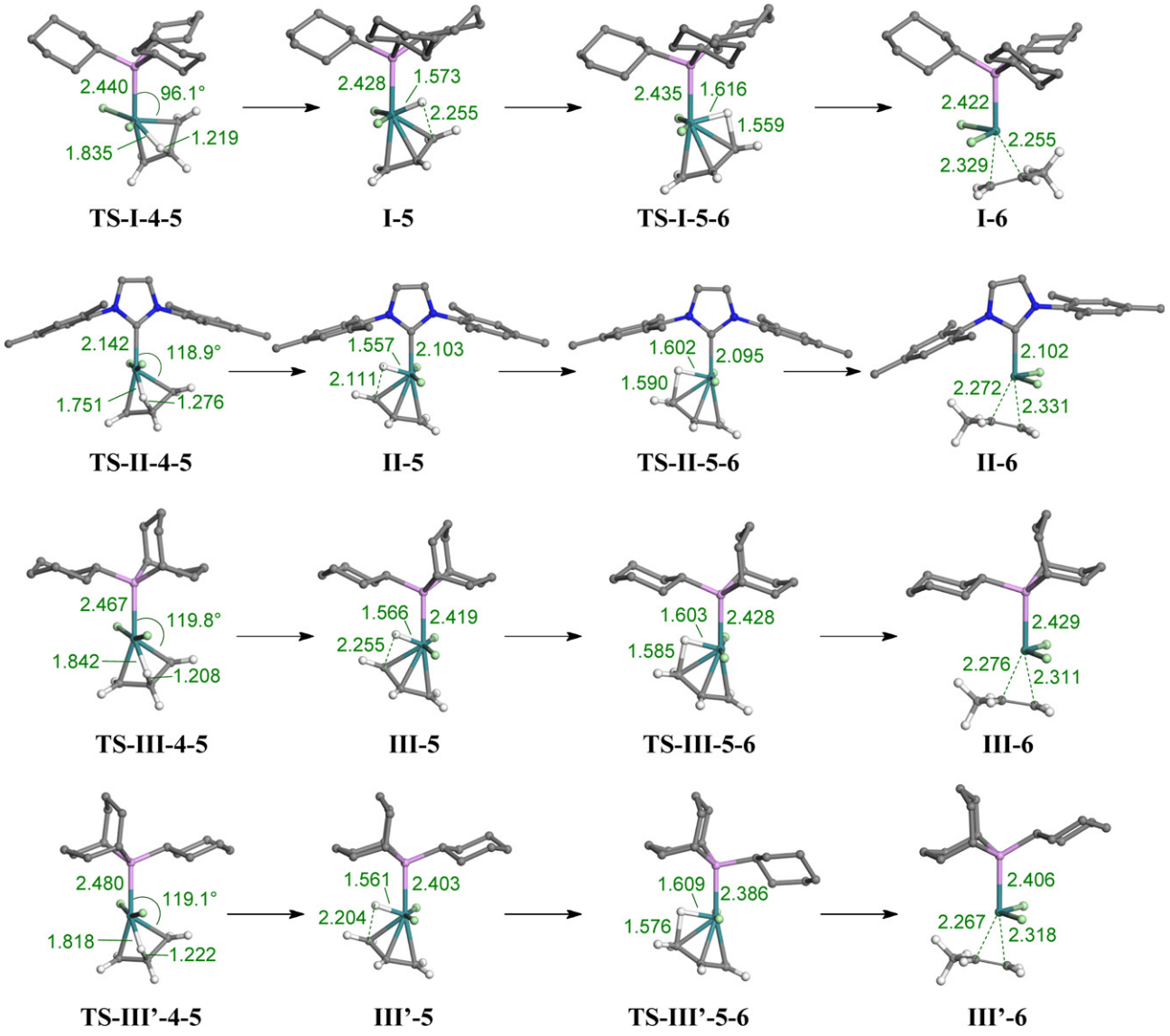

Scheme 3. Optimized geometries for substrate-induced decomposition of ruthenacyclobutanes for the first- and second-generation, as well as Phobcat catalyst models. The selected bond lengths are in angstrom (Å) and hydrogen atoms on the ligands are omitted for clarity.

ΔG_{298}(**II-3c**)] = ~ 6.3 kcal/mol. Also, because the transformation **II-3a** → **II-4** is essentially barrierless the ΔG_{298} energy for **TS-II-3a-4** is also estimated at ~6.3 kcal/mol. This estimate is believed to represent the most accurate relative ΔG_{298} changes for the second-generation catalyst in this region of the free energy surface.

4. Discussion

Catalyst initiation in the commonly accepted dissociative metathesis reaction mechanism involves dissociation of a ligand from the precatalyst complex prior to olefin coordination. Dissociation of PCy_3 from the lowest energy first-generation 16*e* precatalyst complex (**I-1b**) proceeds with $\Delta E = 19.3$ kcal/mol (Table 1). However, the calculated dissociation enthalpy ($\Delta H_{298} = 16.7$ kcal/mol) and entropy ($T\Delta S_{298} = 14.6$ kcal/mol) results in a ΔG_{298} for PCy_3 dissociation of only 2.1 kcal/mol (Fig. 5). It is thus evident that both a favorable enthalpy (compared to ΔE) and entropy contribution, mainly attributed to the generation of two molecules (**I-2b** + PCy_3) from one (**I-1b**), results in an ΔE correction by 17.2 kcal/mol. This correction is in qualitative agreement to ΔG_{298} initiation corrections calculated for the strip-down precatalysts $Cl_2(PH_3)_2Ru{=}CH_2$ and $Cl_2(Pme_3)_2Ru{=}CH_2$[25]. Dissociation of PCy_3 from the second-generation precatalyst (**II-1a**, $\Delta E = 23.8$ and $\Delta G_{298} = 4.6$ kcal/mol) is calculated to be less favourable compared to the first-generation precatalyst. Once again, the ΔH_{298} (21.5 kcal/mol) and $T\Delta S_{298}$ (16.9 kcal/mol) values account for significant correction to ΔE. The relatively less favorable phosphine dissociation for the second-generation catalyst is in agreement with experimental kinetic studies by Grubbs [13,14] in which it was shown that substitution of one PCy_3 ligand in **I** with IMes results in ~640

Table 1
Calculated electronic (ΔE) and Gibbs free energies (ΔG_{298}) at 298.15 K and 1 atm in kcal/mol for the metathesis and decomposition mechanistic sequence **1–6** as catalyzed by the first- (**I**) and second-generation (**II**), as well as Phobcat (**III**) catalysts

	I		**II**		**III**		**III′**	
	ΔE	ΔG_{298}	ΔE	ΔG_{298}	ΔE	ΔG_{298}	ΔE	ΔG_{298}
1a	~6.0[a]	–	0.0	0.0	0.0	0.0	0.5[g]	−0.3
1b	0.0	0.0	5.0	2.9	4.7	6.4	6.2	6.8
2a	–	–	29.0	11.7	–	–	–	–
2b	19.3	2.1	23.8	4.6	25.8	9.6	27.2	10.3
3a	18.6	12.7	~12.1[b]	~6.3[e]	~19.0[f]	–	~19.7[f]	–
3b	13.0	8.1	16.3[c]	9.1	17.9	15.0	19.9	16.4
3c	21.1	15.7	13.2	7.4	17.0	14.8	18.3	15.5
3d	14.2	9.4	17.7	12.8	17.5	15.2	20.2	18.0
TS-3-4	18.4	13.8	~12.1[d]	~6.3[d]	18.4	15.7	19.8	15.9
4	10.9	9.2	1.7	−0.8	8.5	7.5	8.5	7.5
TS-4-5	29.5	26.1	27.2	23.4	28.0	26.6	28.3	26.9
5	−2.0	−3.7	−2.5	−5.1	0.5	−0.8	−0.1	−1.9
TS-5-6	3.0	−0.7	−1.7	−5.3	3.5	1.0	2.8	0.9
6	−4.6	−8.5	−3.3	−7.5	−0.6	−3.0	−1.2	−4.7

All energies are reported relative to the respective catalyst precursor complexes **I-1b**, **II-1a** and **III-1a** and balanced with the energies of free ligand and free ethylene where necessary.

[a] ΔE for flattening of PES during spontaneous optimization to **I-1b**.

[b] ΔE for flattening of PES during spontaneous optimization to **II-4**.

[c] Transition state for methylidene rotation from perpendicular to parallel relative to the Cl–Ru–Cl plane.

[d] **II-3a** → **II-4** proceeds without barrier.

[e] ΔG_{298} is estimated from the Gibbs free energy for formation of **II-3c** according to: ΔE (**II-3a**) − [ΔE(**II-3c**) − ΔG_{298} (**II3c**)].

[f] ΔE for flattening of PES during spontaneous optimization to **III-4**.

[g] All ΔE and ΔG_{298} values for **III′** structures are relative to **III-1a**.

times slower phosphine exchange rate. A similar trend is found for relative first- and second-generation initiation ΔE values calculated in independent BP86 DFT studies on complete catalyst models by Chen [28] and Cavallo [26] in contrast to the reversed trend obtained from B3LYP calculations by Harvey [29]. The dissociation of Phoban-Cy in the Phobcat precatalyst isomers **III-1a** ($\Delta E = 25.8$ and $\Delta G_{298} = 9.6$ kcal/mol) and **III′-1a** ($\Delta E = 26.7$ and $\Delta G_{298} = 10.6$ kcal/mol) is calculated to be less favorable compared to both the first- and second-generation catalysts. This result corroborates the experimental slower initiation kinetics obtained for Phobcat compared to the first- and second-generation catalyst systems [49]. This relatively unfavourable dissociation of a phoban-Cy ligand is attributed to the lower steric congestion experienced by Ru for coordination of phoban-Cy compared to PCy_3, effectively favoring stronger coordination of the phoban-Cy to ruthenium.

The coordination of the model olefinic species, ethylene, to the unsaturated 14*e* complex **2** proceeds with exothermic ΔE changes on the potential energy surface for all the catalysts considered (Table 1). However, the significant loss of translational entropy upon coordination of ethylene to **2** reverses this result, yielding endergonic ΔG_{298} free energy changes in all cases calculated (Table 1 and Fig. 5). In particular, for the first-generation catalyst the most favorable coordination mode of ethylene (**I-2b** + ethylene → **I-3b**) proceeds with an increase in ΔG_{298} of 6.0 kcal/mol, which corresponds to ΔH_{298} and $T\Delta S_{298}$ changes of −5.1 and −11.1 kcal/mol, respectively. This effect is significantly less pronounced for the most likely coordination mode of ethylene to the unsaturated second-generation 14*e* complex (**II-2b** + ethylene → **II-3a**), with ΔG_{298} estimated at 1.7 kcal/mol. Ethylene coordination to the 14*e* electron complexes for the Phobcat isomers proceed both with ΔG_{298} values of 5.2 kcal/mol. This corresponds to $\Delta H_{298} = -6.8$ and $T\Delta S_{298} = -12.0$ kcal/mol (**III-2b** + ethylene → **III-3c**) and $\Delta H_{298} = -7.1$ and $T\Delta S_{298} = -12.2$ kcal/mol (**III′-2b** + ethylene → **III′-3c**), respectively.

Grubbs et al. [13,14,16] have demonstrated that the activity of a metathesis catalyst may be elegantly correlated to the ratio of the rates for phosphine recoordination (k_{-1}) and ethylene coordination (k_2) to the naked 14*e* complex **2**. In particular, it was found that k_{-1}/k_2 is 4 orders of magnitude larger for the first-generation catalyst compared to the second-generation system (with ligand H_2-IMes) quantifying the relative better olefin coordination selectivity versus phosphine coordination for the latter catalyst to its higher experimentally observed activity. Cavallo [26] correlated this experimental trend found for k_{-1}/k_2 with the calculated *difference* in BP86 calculated binding energies for PCy_3 and ethylene to the respective naked 14*e* complexes for first- and second-generation systems. However, we find that the *ratio* of calculated ligand and ethylene binding energies provide for a more appropriate comparison of calculated data with experimentally determined k_{-1}/k_2 trends. Table 2 lists these ratio's for ligand and ethylene binding energies, determined from both ΔE and ΔG_{298}, for the four catalyst species considered in the current study. Note that due to the endergonic nature of ethylene coordination to 14*e* complexes on the ΔG_{298} surface the absolute value for the ΔG_{298} determined ratio's are employed for direct

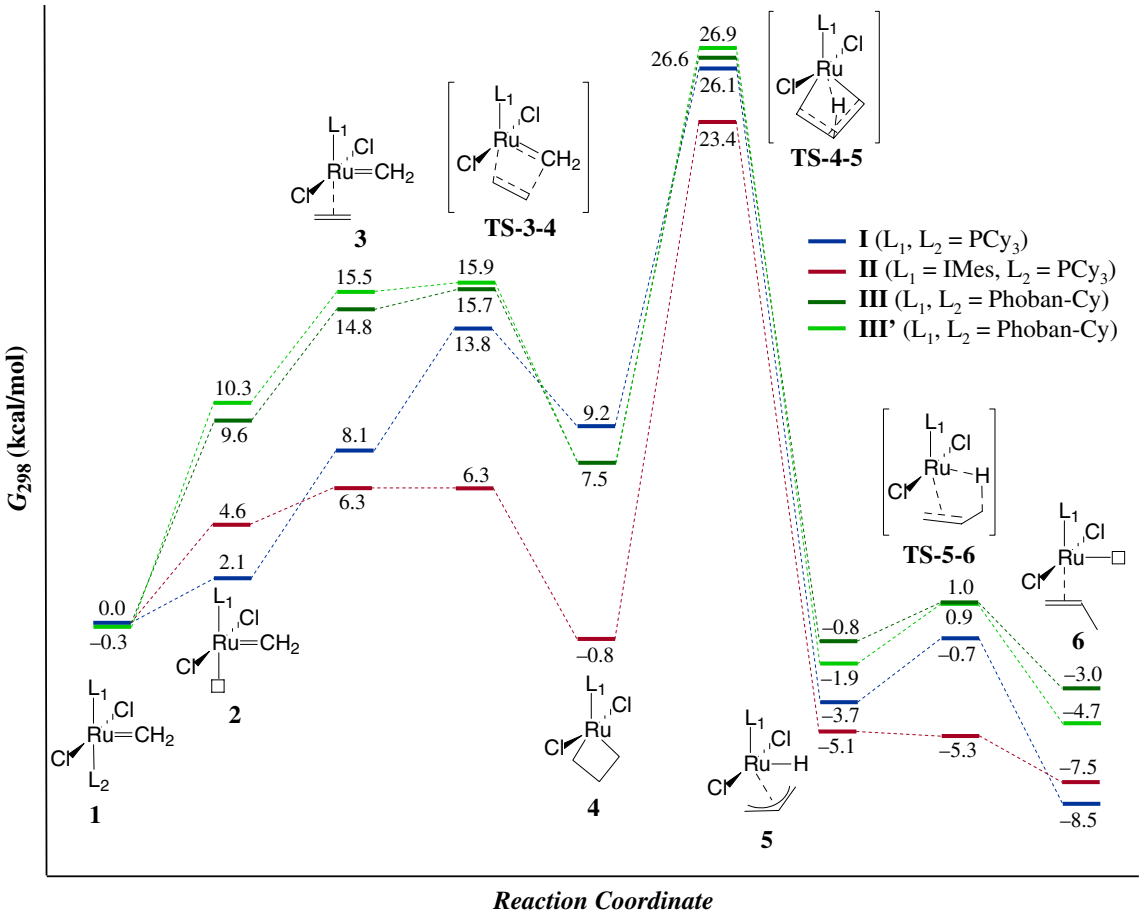

Fig. 5. ΔG_{298} energy surfaces (at 298.15 K and 1 atm in kcal/mol) for the degenerate ethylene metathesis mechanism (**1** ↔ **4**) and substrate-induced decomposition mechanism (**4** → **6**) catalyzed by the first-generation (**I**), second-generation (**II**) and two isomeric Phobcat catalysts (**III** and **III′**), in all cases incorporating the complete ligand systems. Only the energies of the most relevant lowest energy isomers of stationary points are included.

Table 2
Table of calculated ratio's for ligand and ethylene binding energies (for both ΔE and ΔG_{298}), as well as comparative $\Delta G^{\ddagger}_{298}$ and ΔG_{298} energies for selected steps in the **1** → **6** sequence, for **I**, **II**, **III** and **III′**

	I	II	III	III′
Relative ligand versus ethylene coordination				
ΔE ratio	3.06	2.25	2.93	3.06
$\lvert\Delta G_{298}$ ratio$\rvert$	2.86	0.37	0.54	0.49
Ruthenacyclobutane formation (kcal/mol)				
$\Delta G^{\ddagger}_{298}$ (**1** → **4**)	13.8	6.3	15.7	16.2
$\Delta G^{\ddagger}_{298}$ (**2** → **4**)	11.7	1.7	6.1	5.6
$\Delta G^{\ddagger}_{298}$ (**3** → **4**)	5.7	0.0	0.9	0.4
ΔG_{298} (**1** → **4**)	9.2	−0.8	7.5	7.8
ΔG_{298} (**2** → **4**)	7.1	−5.4	−2.1	−2.8
ΔG_{298} (**3** → **4**)	1.1	−7.1	−7.3	−8.0
Allyl hydride formation (kcal/mol)				
$\Delta G^{\ddagger}_{298}$ (**4** → **5**) (kcal/mol)	16.9	24.2	19.1	19.4
ΔG_{298} (**4** → **5**)	−12.9	−4.3	−8.3	−9.4
Ru-propylene complex formation (kcal/mol)				
$\Delta G^{\ddagger}_{298}$ (**5** → **6**)	3.0	−0.2	−1.8	−2.8
ΔG_{298} (**5** → **6**)	−4.8	−2.4	−2.2	−2.8
$\Delta G^{\ddagger}_{298}$ (**6** → **5**)	7.8	2.2	4.0	5.6

comparison to the corresponding ΔE determined ratio's. The preference for ligand binding as apposed to ethylene binding is evident from the calculated ratio's and is summarized for the first- and second-generation catalysts in Table 2, correlating well with the k_{-1}/k_2 trend found experimentally [14]. The difference in ratio between the first- and second-generation systems, determined from the more relevant ΔG_{298} binding energies, is particularly pronounced, mirroring the known higher activity of the latter. It is insightful to note that the $\lvert\Delta G_{298}$ ratio$\rvert$ calculated for each of the two Phobcat isomers is only slightly larger compared to the ratio determined for the second-generation system, effectively predicting that a k_{-1}/k_2 trend for Phobcat will resemble the results reported for the second-generation catalyst rather than the first-generation catalyst (vide infra).

In most theoretical studies reported too date on the metathesis reaction mechanism the formation of the ruthenacyclobutane intermediate from the π-complex (**3**) is calculated to be an equilibrium structure and not a transition state, in accord with a recent ^{13}C labeling NMR study confirming the formation of ruthenacyclobutane

intermediates during metathesis [39]. In fact, most reported theoretical studies reported on full catalyst systems show that the ruthenacyclobutane (**4**) represents the lowest energy intermediate (apart from the precatalyst complex **1**) on the ΔE surface of the active metathesis catalytic cycle [23,28,29], effectively suggesting a relatively larger population of this intermediate during catalysis. Whereas the same result is found in the current study when the ΔE surface is considered (from Table 1 it follows that the ruthenacyclobutane intermediate **4** is only higher in energy compared to the precatalyst complex when ΔE values are compared for all catalysts) a significantly different situation arises when the more relevant ΔG_{298} surface is considered (Fig. 5). From the ΔG_{298} surface plotted in Fig. 5 it follows that for the first-generation catalyst the ruthenacyclobutane (**I-4**) represents the *highest* energy equilibrium stationary point. The calculated reaction free energies for formation of **I-4** form the active 14*e* complex (**I-2b**) and the lowest energy π-complex (**I-3b**) are endergonic by 7.1 and 1.1 kcal/mol, respectively (Table 2). In contrast with this the second-generation ruthenacyclobutane intermediate (**II-4**) represents the *lowest* equilibrium stationary point (for the metathesis sequence **1** ↔ **4**) on the ΔG_{298} surface, even lower than the pre-catalyst complex (**II-1a**) by 0.8 kcal/mol. This amounts to exergonic reaction energies from the corresponding 14*e* complex (**II-2b**) and lowest energy π-complex (**II-3a**) of −5.4 and −7.1 kcal/mol, respectively (Table 2). The calculated relative Gibbs free energies of the Phobcat ruthenacyclobutane intermediates (**III-4** · **III′-4**) is midway between the results described for the first- and second-generation catalysts: **III-4** · **III′-4** is lower in energy than both the 14*e* complexes **III-2b** (by 2.1 kcal/mol) and **III′-2b** (by 2.8 kcal/mol), as well as both the lowest energy π-complexes **III-3c** (by 7.3 kcal/mol) and **III′-3c** (by 8.0 kcal/mol), as summarized in Table 2. The precatalyst complexes **III-1a** and **III′-1a** are, however, lower in energy than the ruthenacyclobutane complex (**III-4**) by 7.5 and 7.8 kcal/mol, respectively (Fig. 5).

In order to achieve a complete picture of relative catalyst activities the activation energies for cyclization of the π-complexes (**3**), to yield the ruthencyclobutane (**4**), need to be considered. However, three different starting points may be considered for interpretation of the activation energies for cyclization, *viz.* the precatalyst complex (**1**), the unsaturated 14*e* complexes (**2**) and the direct reagent π-complexes (**3**). Due to the endergonic nature of the sequence **1** → **2** → **3** → **TS-3-4** (Fig. 5), for all catalysts considered, the total activation barrier for ruthenacyclobutane (**4**) formation may be correlated to the ΔG_{298} change for **1** → **TS-3-4**. The current calculations suggest that these activation energies, listed in Table 2 (**1** → **4**), represent the rate determining step (RDS) for the metathesis sequence **1** ↔ **4**. The largest $\Delta G^{\ddagger}_{298}$ barriers are calculated for the Phobcat isomers **III** (15.7 kcal/mol) and **III′** (16.2 kcal/mol), with the first- (13.8 kcal/mol) and second-generation (6.3 kcal/mol) catalysts exhibiting progressively lower barriers. This suggests relative reaction rates for the three catalysts in decreasing order: second-generation > first-generation > Phobcat. While this theoretical result is in qualitative agreement with preliminary relative turn-over numbers (TOF's) for these three catalysts [50], it should be recognized that initiation and propagation kinetics are not deconvoluted in these calculated $\Delta G^{\ddagger}_{298}$ values.

Alternatively, the 14*e* complexes (**2**) may also be considered as possible starting points for cyclization, because ethylene coordination to **2** is endergonic on the ΔG_{298} surface (Fig. 5), effectively making the π-complexes local minima on the reaction coordinate connecting **2** and the transition structures **TS-3-4**. Both these activation energies (from **2** and **3**) are listed in Table 2 for all the catalyst systems considered. The largest $\Delta G^{\ddagger}_{298}$ values for cyclization are calculated for the first-generation catalyst with barriers from **I-2b** and **I-3b** amounting to 11.7 and 5.7 kcal/mol, respectively. The corresponding $\Delta G^{\ddagger}_{298}$ values for the second-generation catalyst are significantly lower at 1.7 kcal/mol from the 14*e* complex **II-2b** and essentially barrierless transformation from the π-complex **II-3a**. The corresponding activation energies for the Phobcat isomers fits between the $\Delta G^{\ddagger}_{298}$ values calculated for the first- and second-generation systems. The $\Delta G^{\ddagger}_{298}$ values for cyclization from **III-2b** and **III-3c** of 6.1 and 0.9 kcal/mol, respectively, are effectively consistent with the cyclization $\Delta G^{\ddagger}_{298}$ barriers from **III′-2b** and **III′-3c** of 5.6 and 0.4 kcal/mol, respectively. The additional comparison of the reaction energies for **2**, **3** → **4** show in all cases that the Brønsted–Evans–Polanyi relation [51] is obeyed: the more exergonic the reaction energies the lower the corresponding activation energies. In contrast to the results obtained above when the precatalysts are considered as starting points, the following order of relative catalyst activity in decreasing order results: second-generation > Phobcat > first-generation. However, for these relative theoretical activation and reaction energies the relative influence of initiation kinetics are not included.

Although not formally investigated in the current study the effect of ligand rotation during the metathesis mechanism is forthcoming. In order for productive metathesis to proceed from the first-generation ruthenacyclobutane (**I-4**) a rotation of the threefold symmetric PCy_3 ligand through ∼120° was shown from QM/MM calculations by Adlhart and Chen [27] not only to be a prerequisite, but most likely to represent the highest energy barrier for productive degenerate metathesis of styrene with first-generation Ru-benzylidene as catalyst. A similar rotation of the twofold symmetric N-heterocyclic carbene ligand of the second-generation catalyst is not necessary, effectively eliminating an additional rate limiting barrier increase for productive metathesis to proceed. These results led Adlhart and Chen to conclude that the next generation metathesis catalysts are likely to consist of ligands with twofold as apposed to threefold symmetry, effectively eliminating the possibility for differences in barriers for productive and unproductive metathesis (at least for degenerate metathesis) proceeding from a ruthenacyclobutane intermediate. The two isomers of Phobcat (**III** and **III′**) considered in

the current study effectively represent two different ligand orientations, due to the *lack of twofold symmetry* in the phoban-Cy ligand. This rotational behavior leads to interesting conformational complexity of the Phobcat precatalysts, making its characterization significantly more challenging compared to first- and second-generation catalyst systems [44]. This led us to speculate [44] whether the superior catalytic performance of Phobcat is possibly linked to its unique conformational behavior. However, the degenerate and reversible sequence **III-2b** ↔ **III-3c** ↔ **III-4** · **III′-4** ↔ **III′-3c** ↔ **III′-2b**, effectively representing both productive and unproductive metathesis, is calculated to proceed with almost equivalent reaction barriers and activation energies (see Fig. 5 and Table 2) without any ligand rotation required. This is especially evident from the close resemblance of the ΔG_{298} surfaces illustrated for **III** and **III′** in Fig. 5. It can thus be concluded that although the ligand in Phobcat does not formally have twofold symmetry, it acts like a ligand with twofold symmetry independent of the orientation of the ligand. This, in combination with the relatively favorable competition of olefin coordination versus ligand recoordination to the unsaturated 14*e* complex, establish the similarity of the Phobcat catalyst to the second-generation catalyst.

In order to appropriately correlate the relative experimental determined conversions for first- and second-generation and Phobcat both the reactivities and stabilities of the catalysts need to be considered. We recently predicted and confirmed substrate-induced decomposition of first- and second-generation catalysts, involving the formation of Ru-propene complexes during degenerate ethylene metathesis with the corresponding Ru-methylidene complexes [38]. Propylene formation during the degenerate metathesis of ethylene was also later confirmed by ^{13}C labeling studies by Romero and Piers [39]. The mechanism involves the decomposition of a ruthenacylobutane intermediate (**4**) via β-hydride transfer to yield the corresponding allyl hydride complex (**5**). Subsequent reductive elimination of propylene proceeds through further hydride transfer to a terminal allyl carbon in **5**, liberating a Ru-propylene complex (**6**) which is inactive for metathesis. The DFT calculated mechanistic details of this decomposition route for the first- and second-generation catalyst was already reported elsewhere [38] and is thus only included in the current study to afford direct comparison with additional results obtained for this decomposition route for Phobcat. Whereas it is agreed that the decomposition of Ru-alkylidene complexes most likely proceeds via a number of different decomposition routes, this substrate-induced decomposition mechanism was included in the current study as a representative decomposition mechanism under catalytic conditions to afford direct comparison with the basic metathesis mechanistic steps. From Fig. 5 it follows that the rate limiting step for this decomposition route, for all four catalyst models considered, involves the formation of the allyl hydride species (**5**) from the corresponding ruthenacyclobutane (**4**). The calculated $\Delta G^{\ddagger}_{298}$ barrier and ΔG_{298} reaction energy for the formation of **I-5** from **I-4** for the first-generation catalyst are 16.9 and −12.9 kcal/mol, respectively (Table 2). In contrast, the corresponding barrier and reaction energy for the second generation catalyst (**II-4** → **II-5**) are significantly less favorable at 24.2 and −4.3 kcal/mol, respectively. The calculated $\Delta G^{\ddagger}_{298}$ barriers for Phobcat ruthenacyclobutane **III-4** (equivalent to **III′-4**) conversion to **III-5** and **III′-5** are 19.1 and 19.4 kcal/mol, respectively, while the corresponding ΔG_{298} reaction energies are −8.3 and −9.4 kcal/mol, respectively (Table 2). Based on both kinetic and thermodynamic grounds it is thus concluded that the prevalence for substrate-induced decomposition in the catalysts considered follows the trend: first-generation > Phobcat > second-generation in decreasing order. These results are in quantitative agreement with a higher observed propensity for the first-generation catalyst to form propylene compared to Phobcat under conditions of degenerate ethylene metathesis [52]. Also, the known higher stability of the second-generation catalyst is also reflected in this data.

Lastly, the nature of the relative ΔG_{298} surfaces for reduction of the allyl hydride species (**5**) to the corresponding Ru-propylene complexes (**6**) is noteworthy (Fig. 5). Propene formation from the first-generation (**I-5**) and Phobcat (**III-5** and **III′5**) allyl hydride complexes proceeds with $\Delta G^{\ddagger}_{298}$ barriers of 1.8–3.0 kcal/mol compared to an essentially barrierless transformation for the second-generation catalyst (Table 2). The relatively low $\Delta G^{\ddagger}_{298}$ barrier for the reverse reaction (**6** → **5**) for the second-generation system (2.2 kcal/mol) compared to the first-generation (7.8 kcal/mol) and Phobcat (4.0 and 5.6 kcal/mol, respectively) systems, suggests more favorable reversible allyl hydride formation from Ru-olefin π-complexes containing N-heterocyclic carbene ligands compared to Ru-phosphine complexes. Although not necessarily linked to the substrate-induced decomposition mechanism described here, this relatively reversible formation of Ru-allyl hydride ↔ Ru-olefin π-complexes may represent a viable olefin isomerization mechanism, correlating the known propensity of second-generation catalysts to afford secondary metathesis products (SMP's), in contrast to both the first-generation and Phobcat catalysts. An allyl-type isomerization mechanism was also proposed by Nolan et al. [8], while the propensity of Ru-hydride complexes to act as olefin isomerization catalysts is well-known [9,53].

5. Conclusion

Complete DFT calculated Gibbs free energy surfaces for the basic metathesis mechanism of three ruthenium catalysts, *viz.* first- and second-generation catalysts and the recently developed Phobcat catalyst are constructed and compared in the current study. The models incorporate the full ligands as used in experiment, while ethylene and Ru-methylidene were used as models for olefin substrate and alkylidene, respectively. From the calculations correlations to experimentally observed reactivity trends are

made. In particular, catalyst initiation behavior is accurately reproduced from the calculated ligand dissociation free energy changes, confirming the relatively fast initiation of first-generation systems with progressively slower initiation for the second-generation and Phobcat catalysts. Good correlation of the experimentally determined ratio of the rate of ligand recoordination and ethylene coordination, k_{-1}/k_2, with the calculated ratio's of ligand and ethylene binding energies to unsaturated 14*e* complexes is found for the first- and second-generation catalysts, while an intermediate trend is predicted for Phobcat. Analyses of $\Delta G^{\ddagger}_{298}$ barriers and ΔG_{298} reaction energies for ruthenacyclobutane formation from different precursor complexes, i.e. precatalyst, 14*e* unsaturated complex and ethylene coordinated π-complex, provide for fundamental insight into the relative reactivities of the three catalysts studied. Furthermore, the relative increase in the rate determining ruthenacyclobutane formation barrier due to a prerequisite rotation of the threefold symmetric ligand of traditional first-generation catalysts is shown not to be necessary for the phoban-Cy ligand of Phobcat. Instead, the ligand of Phobcat is shown to act like a second-generation twofold symmetric ligand, despite not having formal twofold symmetry. From this data important general insight is gained into the requirements for the development of new ligands for improved reactivity in Ru-catalyzed olefin metathesis.

In addition, a detailed comparison of substrate-induced decomposition of Phobcat versus the first- and second-generation catalysts is presented. The incorporation of this decomposition mechanistic data facilitates a more complete correlation of experimental reactivity data with both calculated catalyst activity trends and calculated catalyst stability. It is shown, for example, that the substrate-induced decomposition propensity follows the increasing order: second-generation < Phobcat < first-generation, in agreement with experimental observation. Possible insight into the importance of Ru-allyl hydride complexes responsible for olefin isomerization side reactions during second-generation catalyzed olefin metathesis is also gained from the construction of the decomposition ΔG_{298} surfaces.

Acknowledgements

We thank the Sasol Homogeneous Metathesis Group for valuable discussions, Mr. Ivan Bester (Information Management, Sasol) for infrastructure support to the Sasol Molecular Modeling Group, Dr. Jan-Albert van den Berg for his input in preparing the final manuscript and Sasol Technology Research and Development for permission to publish this work.

References

[1] For recent reviews on olefin metathesis see: (a) R.H. Grubbs (Ed.), Handbook of Metathesis, Wiley-VCH, Weinheim, Germany, 2003;
(b) S. Mecking, A. Held, F.M. Bauers, Angew. Chem., Int. Ed. 41 (2002) 544;
(c) G.W. Coates, J. Chem. Soc., Dalton Trans. (2002) 467;
(d) S.J. Connon, S. Blechert, Angew. Chem., Int. Ed. 42 (2003) 1900;
(e) J.C. Mol, J. Mol. Catal. A: Chem. 213 (2004) 39;
(f) R.H. Grubbs, D.M. Lynn, Aquous-Phase Organometallic Catalysis, 2nd ed., Wiley-VCH, 2004, pp. 550–566;
(g) D. Astruc, New J. Chem. 29 (2005) 42.

[2] (a) Y. Chauvin, Angew. Chem., Int. Ed. 45 (2006) 3740;
(b) R.R. Schrock, Angew. Chem., Int. Ed. 45 (2006) 3748;
(c) R.H. Grubbs, Angew. Chem., Int. Ed 45 (2006) 3760.

[3] (a) S.T. Nguyen, R.H. Grubbs, J.W. Ziller, J. Am. Chem. Soc. 115 (1993) 9858;
(b) P. Schwab, M.B. France, J.W. Ziller, R.H. Grubbs, Angew. Chem., Int. Ed. 34 (1995) 2039;
(c) P. Schwab, R.H. Grubbs, J.W. Ziller, J. Am. Chem. Soc. 118 (1996) 100;
(d) E.L. Dias, S.T. Nguyen, R.H. Grubbs, J. Am. Chem. Soc. 119 (1997) 3887;
(e) H.E. Blackwell, D.J. O'Leary, A.K. Chatterjee, R.A. Washenfelder, D.A. Bussmann, R.H. Grubbs, J. Am. Chem. Soc. 122 (2000) 58.

[4] (a) T. Weskamp, W.C. Schattenmann, M. Speigler, W.A. Herrmann, Angew. Chem., Int. Ed. 37 (1998) 2490;
(b) T. Weskamp, F.J. Kohl, W. Hieringer, D. Gleich, W.A. Herrmann, Angew. Chem., Int. Ed. 38 (1999) 2416;
(c) L. Ackermann, A. Fürstner, T. Weskamp, F.J. Kohl, W.A. Herrmann, Tetrahedron Lett. 40 (1999) 4787;
(d) T. Weskamp, F.J. Kohl, W.A. Herrmann, J. Organomet. Chem. 582 (1999) 362;
(e) U. Frenzel, T. Weskamp, F.J. Kohl, W.C. Schattenmann, O. Nuyken, W.A. Herrmann, J. Organomet. Chem. 586 (1999) 263;
(f) M. Scholl, T.M. Trnka, J.P. Morgan, R.H. Grubbs, Tetrahedron Lett. 40 (1999) 2247;
(g) M. Scholl, S. Ding, C.W. Lee, R.H. Grubbs, Org. Lett. 1 (1999) 953;
(h) J. Huang, E.D. Stevens, S.P. Nolan, J.L. Petersen, J. Am. Chem. Soc. 121 (1999) 2674;
(i) L. Jafarpour, J. Huang, E.D. Stevens, S.P. Nolan, Organometallics 18 (1999) 3760.

[5] (a) For selected examples, see: M. Rosillo, G. Dominguez, L. Casarrubios, U. Amador, J. Perez-Castells, J. Org. Chem. 69 (2004) 2084;
(b) Y. Matsuya, T. Kawaguchi, H. Nemoto, Org. Lett. 5 (2003) 2939;
(c) S. Hanessian, R. Margarita, A. Hall, S. Johnstone, M. Tremblay, L. Parlanti, J. Am. Chem. Soc. 124 (2002) 13342;
(d) M. Mori, K. Tonogaki, N.J. Nishiguchi, J. Org. Chem. 67 (2002) 224;
(e) S.D. Edwards, T. Lewis, R.J.K. Taylor, Tetrahedron Lett. 40 (1999) 4267;
(f) K.C. Nicolaou, N.P. King, Y. He, Topics in Organometallic Chemistry vol. 1 (Alkene Metathesis in Organic Synthesis) (1998) 73–104;
(g) M. Schuster, S. Blechert, Transition Metals for Organic Synthesis 1 (1998) 275.

[6] G.S. Forman, A.E. McConnell, M.J. Hanton, A.M.Z. Slawin, R.P. Tooze, W. Janse van Rensburg, W.H. Meyer, C.L. Dwyer, M.M. Kirk, D.W. Serfontein, Organometallics 23 (2004) 4824.

[7] (a) J. Huang, E.D. Stevens, S.P. Nolan, J.L. Peterson, J. Am. Chem. Soc. 121 (1999) 2674;
(b) M. Scholl, T.M. Trnka, J.P. Morgan, R.H. Grubbs, Tetrahedron Lett. 40 (1999) 2247;
(c) A. Fürstner, O.R. Thiel, L. Ackermann, H.-J. Schanz, S.P. Nolan, J. Org. Chem. 65 (2000) 2204;
(d) J. Wagner, L.M. Martin Cabrejas, C.E. Grosssmith, C. Papageorgiou, F. Senia, D. Wagner, J. France, S.P. Nolan, J. Org. Chem. 65 (2000) 9255;
(e) S.S. Kinderman, J.H. van Maarseveen, H.E. Schoemaker, H. Hiemstra, F P.J.T. Rutjes, Org. Lett. 13 (2001) 2045;
(f) S.E. Lehman Jr., J.E. Schwendeman, P.M. O'Donnell, K.B. Wagener, Inorg. Chim. Acta 345 (2003) 190;
(g) M. Arisawa, Y. Terada, K. Takahashi, M. Nakagawa, A. Nishida, J. Org. Chem. 71 (2006) 4255.

[8] D. Bourgeois, A. Pancrazi, S.P. Nolan, J.J. Prunet, Organomet. Chem. 643–644 (2002) 247.
[9] U.L. Dharmasena, H.M. Foucalt, E.N. dos Santos, D.E. Fogg, S.P. Nolan, Organometallics 24 (2005) 1056.
[10] G.S. Forman, A.E. McConnell, R.P. Tooze, W. Janse van Rensburg, W.H. Meyer, M.M. Kirk, C.L. Dwyer, D.W. Serfontein, Organometallics 24 (2005) 4528.
[11] W.H. Meyer, A.E. McConnell, G.S. Forman, C.L. Dwyer, M.M. Kirk, E.L. Ngidi, A. Blignaut, D. Saku, A.M.Z. Slawin, Inorg. Chim. Acta 359 (2006) 2910.
[12] E.L. Dias, S.T. Nguyen, R.H. Grubbs, J. Am. Chem. Soc. 119 (1997) 3887.
[13] M.S. Sanford, M. Ulman, R.H. Grubbs, J. Am. Chem. Soc. 123 (2001) 749.
[14] M.S. Sanford, J.A. Love, R.H. Grubbs, J. Am. Chem. Soc. 123 (2001) 6543.
[15] M. Ulman, R.H. Grubbs, Organometallics 17 (1998) 2484.
[16] J.A. Love, M.S. Sanford, M.W. Day, R.H. Grubbs, J. Am. Chem. Soc. 125 (2003) 10103.
[17] (a) C. Hinderling, C. Adlhart, P. Chen, Angew. Chem., Int. Ed. 37 (1998) 2685;
(b) C. Adlhart, P. Chen, Helv. Chim. Acta 83 (2000) 2192;
(c) C. Adlhart, M.A.O. Volland, P. Hofmann, P. Chen, Helv. Chim. Acta 83 (2000) 3306;
(d) C. Adlhart, P. Chen, Helv. Chim. Acta 86 (2003) 941;
(e) C. Adlhart, C. Hinderling, H. Baumann, P. Chen, J. Am. Chem. Soc. 122 (2000) 8204;
(f) M.A.O. Volland, C. Adlhart, C.A. Kiener, P. Chen, P. Hoffmann, Chem. Eur. J. 7 (2001) 4621.
[18] (a) K. Basu, J.A. Cabral, L.A. Paquette, Tetrahedron Lett. 43 (2002) 5453;
(b) J.A. Tallarico, P.J. Bonitatebus, M.L. Snapper, J. Am. Chem. Soc. 119 (1997) 7157;
(c) W. Stüer, J. Wolf, H. Werner, J. Organomet. Chem. 641 (2002) 203;
(d) S.E. Lehman, K.B. Wagener, Macromolecules 35 (2002) 48.
[19] (a) M.T. Benson, T.R. Cundari, Int. J. Quant. Chem. 65 (1997) 987;
(b) G.J. Spivak, J.N. Caulter, M. Olivan, O. Eisenstein, K.G. Caulton, Organometallics 17 (1998) 999;
(c) S.M. Hansen, F. Rominger, M. Metz, P. Hoffmann, Chem. Eur. J. 5 (1999) 557;
(d) T. Weskamp, F.J. Kohl, W. Hieringer, D. Gleich, W.A. Herrmann, Angew. Chem., Int. Ed. 38 (1999) 2416;
(e) F. Bernardi, A. Bottoni, G.P. Miscione, Organometallics 19 (2000) 5529;
(f) S.F. Vyboishchikov, M. Bühl, W. Thiel, Chem. Eur. J. 8 (2002) 3962;
(g) F. Bernardi, A. Bottoni, G.P. Miscione, Organometallics 22 (2003) 940;
(h) I.T. Sabbagh, P.T. Kaye, J. Mol. Struct. Theochem. 763 (2006) 37.
[20] C.H. Suresh, N. Koga, Organometallics 23 (2004) 76.
[21] (a) O.M. Aagaard, R.J. Meier, F. Buda, J. Am. Chem. Soc. 120 (1998) 7174;
(b) R.J. Meier, O.M. Aagaard, F. Buda, J. Mol. Catal. A: Chem. 160 (2000) 189.
[22] J. Lippstreu, B.F. Straub, J. Am. Chem. Soc. 127 (2005) 7444.
[23] M. Jordaan, P. van Helden, C.G.C.E. van Sittert, H.C.M. Vosloo, J. Mol. Catal. A: Chem. 254 (2006) 145.
[24] K.A. Burdett, L.D. Harris, P. Margl, B.R. Maughon, T. Mokhtar-Zadeh, P.C. Saucier, E.P. Wasserman, Organometallics 23 (2004) 2027.
[25] S. Fomine, S.M. Vargas, M.A. Tlenkopatchev, Organometallics 22 (2003) 93.
[26] L. Cavallo, J. Am. Chem. Soc. 124 (2002) 8965.
[27] C. Adlhart, P. Chen, Angew. Chem., Int. Ed. 41 (2002) 4484.
[28] C. Adlhart, P. Chen, J. Am. Chem. Soc. 126 (2004) 3496.
[29] A.C. Tsipis, A.G. Orpen, J.N. Harvey, Dalton Trans. (2005) 2849.
[30] (a) A.C. Hillier, W.J. Sommer, B.S. Yong, J.L. Peterson, L. Cavallo, S.P. Nolan, Organometallics 22 (2003) 4322;
(b) S. Gatard, S. Kahlal, D. Méry, S. Nlate, E. Cloutet, J.-Y. Saillard, D. Astruc, Organometallics 23 (2004) 1313;
(c) C. Costabile, L. Cavallo, J. Am. Chem. Soc. 126 (2004) 9592.
[31] (a) D. Benitez, W.A. Goddard, J. Am. Chem. Soc. 127 (2005) 12218;
(b) S.F. Vyboishchikov, W. Thiel, Chem. Eur. J. 11 (2005) 3921;
(c) S. Fomine, J.V. Ortega, M.A. Tlenkopatchev, Organometallics 24 (2005) 5696.
[32] G. Occhipinti, H.-R. Bjørsvik, V.R. Jensen, J. Am. Chem. Soc. 128 (2006) 6952.
[33] J.L. Hérisson, Y. Chauvin, Makromol. Chem. 141 (1971) 161.
[34] M. Ulman, R.H. Grubbs, J. Org. Chem. 64 (1999) 7202.
[35] S.H. Hong, M.W. Day, R.H. Grubbs, J. Am. Chem. Soc. 126 (2004) 7414.
[36] D. Amoroso, G.P.A. Yap, D.E. Fogg, Organometallics 21 (2002) 3335.
[37] D. Amoroso, G.P.A. Yap, D.E. Fogg, Can. J. Chem. 79 (2001) 958.
[38] W. Janse van Rensburg, P.J. Steynberg, W.H. Meyer, M.M. Kirk, G.S. Forman, J. Am. Chem. Soc. 126 (2004) 14332.
[39] P.E. Romero, W.E. Piers, J. Am. Chem. Soc. 127 (2005) 5032.
[40] For related transformations on substituted metallocyclobutanes see:
(a) C. Pietrazuk, H. Fischer, Chem. Commun. (2000) 2463;
(b) K. McNeill, R.A. Andersen, R.G. Bergman, J. Am. Chem. Soc. 117 (1995) 3625;
(c) C. Slugovc, K. Mereiter, R. Schmid, K. Kirchner, J. Am. Chem. Soc. 120 (1998) 6175;
(d) C. Slugovc, K. Mereiter, R. Schmid, K. Kirchner, Eur. J. Inorg. Chem. (1999) 1141;
(e) C. Six, K. Beck, A. Wegner, W. Leitner, Organometallics 19 (2000) 4639.
[41] For related transformations on other metallacyclobutanes see: (a) S.J. McLain, C.D. Wood, R.R. Schrock, J. Am. Chem. Soc. 99 (1977) 3519;
(b) M.J. Szabo, H. Berke, T. Weiss, T. Ziegler, Organometallics 22 (2003) 3671.
[42] (a) B. Delley, J. Chem. Phys. 92 (1990) 508;
(b) B. Delley, J. Phys. Chem. 100 (1996) 6107;
(c) B. Delley, J. Chem. Phys. 113 (2000) 7756.
[43] J.P. Perdew, Y. Wang, Phys. Rev. B45 (1992) 13244.
[44] C.L. Dwyer, M.M. Kirk, W.H. Meyer, W. Janse van Rensburg, G.S. Forman, Organometallics 25 (2006) 3806.
[45] For use with cobalt see: (a) C. Crause, L. Bennie, L. Damoense, C.L. Dwyer, C. Grove, N. Grimmer, W. Janse van Rensburg, M.M. Kirk, K. Mokheseng, S. Otto, P.J. Steynberg, Dalton Trans. (2003) 2036;
For use with chromium see: (b) W. Janse van Rensburg, C. Grove, J.P. Steynberg, K.B. Stark, J.J. Huyser, P.J. Steynberg, Organometallics 23 (2004) 1207.
[46] B. Delley, in: J.M. Seminario, P. Politzer (Eds.), Modern Density Functional Theory: A Tool for Chemistry, Theoretical and Computational Chemistry, vol. 2, Elsevier, Amsterdam, The Netherlands, 1995.
[47] J. Andzelm, R.D. King-Smith, G. Fitzgerald, Chem. Phys. Lett. 335 (2001) 321.
[48] It should be noted that due to the symmetry of the Phobcat ruthenacyclobutane intermediate, **III-4** and **III′-4** are equivalent.
[49] Preliminary 1H NMR phosphorous exchange studies are in agreement with the calculated results. It should further be noted that: (i) Phobcat is directly synthesized from the first-generation (PCy_3) catalyst, effectively suggesting higher coordination energies for Phoban-Cy compared to PCy_3 (Phoban-Cy concentration is higher than PCy3 concentration, however); and (ii) catalysis with Phobcat is initially slower compared to the first-generation catalyst.
[50] Unpublished experimental results show that Phobcat achieves the slowest TOF of 200 min^{-1} in the solvent-free metathesis of 1-octene (50 °C), while the first- and second-generation catalysts reach 300 min^{-1} and 1700 min^{-1}, respectively (1-octene: Ru = 9000, but

18000 for the latter). While the traditional Grubbs catalysts do not show a sign of initiation under these conditions, the S-shaped curve of the plot of product formation over time clearly indicates for Phobcat the slower transformation of the starting benzylidene complex to an alkylidene in the catalytic cycle. Accordingly, the fastest TOF is reached within the first minute for the two Grubbs catalysts and only around 3–5 min for Phobcat.

[51] (a) J.N. Brønsted, Chem. Rev. 5 (1928) 231;
(b) M.G. Evans, N. Polanyi, Trans. Faraday Soc. 32 (1936) 1333.
[52] These calculations have been confirmed experimentally by preliminary 1H NMR studies. Full details of these studies will be disclosed in due course.
[53] A. Fürstner, L. Ackermann, B. Gabor, R. Goddard, C.W. Lehman, R. Mynott, F. Stelzer, O.R. Thiel, Chem. Eur. J. 7 (2001) 3236.